Measurement of Indoor Channel Characteristics At 20 GHz Band

Ngochao Tran, Tetsuro Imai, and Yukihiko Okumura
NTT DOCOMO, INC.
3-6 Hikari-no-oka, Yokosuka-shi, Kanagawa-ken 239-8536 Japan
e-mail: ngochao.tran.fr@nttdocomo.com

***Abstract*— A high frequency (over 6 GHz) band 5G system with a very high data transmission rate has been the focus of studies recently. One important issue to enable this system is clarifying the propagation characteristics at high frequency (over 6 GHz) bands. This paper presents the channel characteristics at the 20 GHz band for an indoor office environment. Measurements are performed using a channel sounder at the 20 GHz band with a 50-MHz-bandwidth orthogonal frequency-division multiplexing signal. A 19 dBi horn antenna is rotated in azimuth and elevation on the receiver side in order to measure the Power Delay Profile (PDP) at each angle. By combining all the PDPs, the channel characteristics are estimated as if using an omni-directional antenna. The measured and estimated results show that the path loss values are lower than those in free space. The averages of the delay spread, azimuth angle spread, and elevation angle spread are 60.4 ns, 64.7 degrees, and 3.6 degrees, respectively. The standard deviations of the delay spread, azimuth angle spread, and elevation angle spread are 9.7 ns, 10.7 degrees, and 3.1 degrees, respectively.**

Keywords—5G, high frequency (over 6 GHz) bands, indoor channel characteristics.

I. INTRODUCTION

In recent years, due to the popular use of mobile phones and in particular smartphones, the amount of mobile data traffic has increased at an explosive rate. To address this trend, the 5G system, which enables data transmission at a high bit rate and is based on the "phantom cell concept" was proposed [1]. In this system, small cells (including indoor hotspots) with high bit rate communications are overlaid onto macrocells, which secure coverage and mobility. Ultra-high frequency (UHF) bands are used for macrocells. Super high frequency (we consider frequencies over 6 GHz and refer to them as high-SHF) and extremely high frequency (EHF) bands are applied to the small cells in order to obtain wider bandwidths. Considering a scenario using high-SHF and EHF bands for an indoor hotspot, to design radio links with high accuracy, the channel characteristics such as path loss, delay spread, and angle spread, must be clarified. In order to choose appropriate carrier frequencies, the channel characteristics at various high frequency (over 6 GHz) bands should be investigated.

Recently, many studies on indoor channel characteristics around the 60 GHz band have been reported [2]-[7]. In addition, some measurements and analyses at the 10 GHz, 11 GHz, and 28 GHz bands have been conducted [8]-[12]. However, to the best knowledge of the authors, only few measurements and analyses of indoor channel characteristics at other high frequency bands have been reported. Therefore, it is necessary to clarify indoor channel characteristics at other high frequency bands.

In this paper, we present channel characteristics such as path loss, delay spread, angle spread in an indoor office environment at the 20 GHz band. The measurements are conducted in a typical office using a channel sounder with a 50 MHz bandwidth. A 19 dBi horn antenna is rotated in azimuth and elevation on the receiver side in order to measure the Power Delay Profile (PDP) at each angle. After combining all the measured PDPs, the channel characteristics are estimated as if using an omni-directional antenna on the receiver side.

II. MEASUREMENT SYSTEM AND ENVIRONMENT

A. Channel Sounder for 20 GHz band

Fig. 1 shows the configuration and Table I gives the specifications for the channel sounder for the 20 GHz band. On the transmitter side, orthogonal frequency-division multiplexing (OFDM) signals with a 50 MHz bandwidth at the 20 GHz band are generated and propagated into the air using a 2.4 dBi sleeve antenna. The transmission power is 30 dBm. On the receiver side, a 19.1 dBi horn antenna with a 20 degree half-power beamwidth is used to receive the radio frequency (RF) signals. After down-converting the RF signals to an intermediate frequency (IF) band, the complex amplitudes of

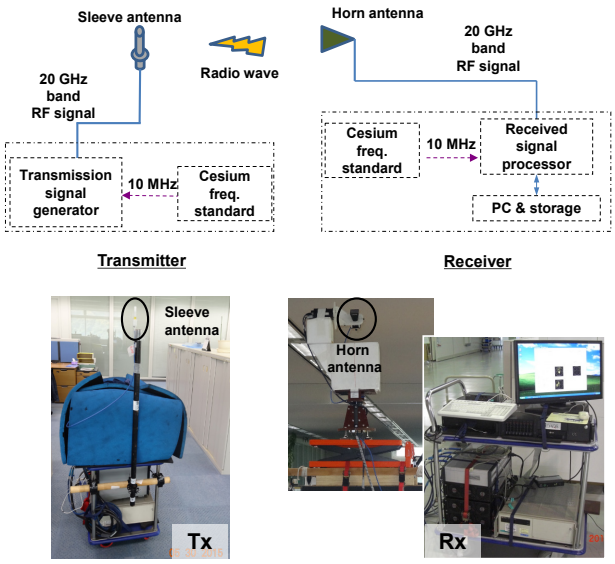

Fig. 1. Configuration of channel sounder for 20 GHz band.

TABLE I. CHANNEL SOUNDER SPECIFICATIONS

Center frequency	19.85 GHz
Bandwidth	50 MHz
Transmission signal	OFDM
Number of subcarriers	449
Transmission power	30 dBm
Tx antenna	Sleeve (2.4 dBi)
Rx antenna	Horn (19.1dBi: 20 deg. HPBW)

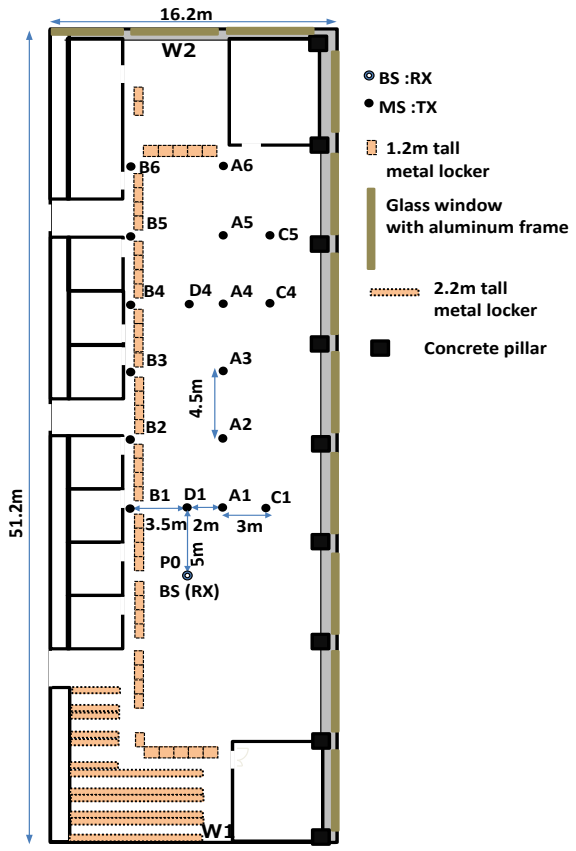

Fig. 2. Indoor office environment.

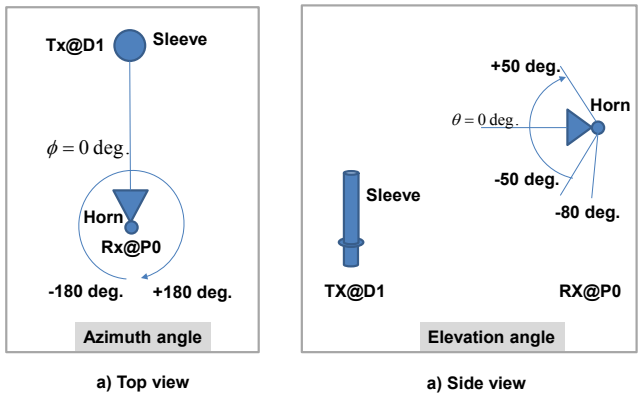

Fig. 3. Definition of azimuth /elevation angle at BS.

the subcarriers (transfer functions) are stored in a PC. The PDPs are obtained by converting stored data into channel impulse responses.

B. Measurement Environment

Fig. 2 shows the indoor office environment used in the measurements. The office size is 51.2 m × 16.2 m × 2.7 m. There are wooden desks and drawers, chairs, and metal lockers arranged in the office. There are also some meeting rooms and office equipment rooms that are surrounded by glass with metal frames and metal doors. The windows are glass with aluminum frames. Near by the windows, there are some concrete pillars.

III. MEASUREMENTS AND ANALYSIS PROCEDURE

In order to measure the channel characteristics at a base station (BS), we located the transmitter (Tx) of the channel sounder at points A1-A6, B1-B6, C1, C4, C5, D1, and D4 as shown in Fig. 2. The height of the sleeve antenna is 1.5 m. The receiver (Rx) of the channel sounder is located at point P0 at the antenna height of 2.3 m. At each Tx location, we rotated the horn antenna in azimuth and elevation and measured five PDPs at each angle combination on the Rx side. At A3, the azimuth angle of the horn antenna is changed from -180 degrees to +180 degrees in 1 degree steps, and the elevation angle is changed from -80 degrees to +50 degrees in 1 degree steps. For the other Tx locations, the range and resolution of the azimuth angle is not changed, but the elevation angle is changed from -50 degrees to +50 degrees in 10 degree steps. Here, the azimuth angle and elevation angle of the horn antenna are defined as shown in Fig. 3. There were no people moving in the office during the measurements. The measurements are performed automatically.

In order to detect delay times and angles of arrival of paths with high accuracy, we processed the PDPs using the steps described hereafter.

1) Combine PDPs: At each Tx location and each elevation angle, we combined all PDPs in azimuth and obtained a 3D (azimuth, delay, power) PDP.

2) Cut noise floor: At each Tx location, the maximum power value, *MaxP,* of the 3D PDPs is detected first. Because the dynamic ranges of the measured PDPs in terms of the delay time are greater than 35 dB, only the PDPs that have a relative power greater than -35 dB compared to the *MaxP* are considered.

3) Decoupling horn angle pattern: For each delay time point, t_i, of the 3D PDPs, we searched for the maximum power value, $MaxP_{i,}$ in azimuth. Because the relative level of the side lobe of the horn antenna is -33 dB, only the PDPs that have a relative power greater than -30 dB compared to the $MaxP_i$ are considered.

4) Search peaks (paths): We search the peaks (paths) in two dimensions, i.e., azimuth angle and delay time. If there are multiple peaks in azimuth at the same delay time and the difference in the angles between them is less than 20 degrees of the half power beamwidth of the horn antenna, we select

only the peak that has the maximum power value and do not consider the others peaks.

5) Search peaks with high time resolution: After obtaining the azimuth angles and delay times of the peaks, we focused on the PDPs at each azimuth angle. Because of the sampling time, the delay times of the peaks maybe not be sampled exactly. To obtain more accurate delay times for the peaks, we added the phase shift of $\exp(-j2\pi f_i \Delta)$ to the measured data (complex amplitudes of subcarriers) and converted the values to the time domain to obtain new PDPs. Here, f_i is a subcarrier, and Δ is the shift time. This operation is nearly equal to sampling the received signal with the difference timing of Δ. By varying the value of Δ and comparing the values of the new peaks to those for the original peaks, we could select the peaks with the maximum power values and new delay time. Thus, we obtained the peaks (paths) with high time resolution.

6) Search peaks in elevation angle direction: After searching for peaks with a high time resolution, we searched for peaks in the elevation angle direction by comparing the peaks of each elevation angle and finding the maximum value. Thus, we obtained the elevation angles of the peaks.

IV. MEASUREMENT RESULTS

Fig. 4 shows the received power at the BS corresponding to each combination of the azimuth/elevation angles, when the Tx is located at A3. Here, in order to obtain the received power, five PDPs are averaged and integrated. Based on Fig. 4, we verify that there are some strong paths. By matching the arrival angles to the layout of the office, which is shown in Fig. 2, we know where these paths are reflected. For example, the path with -175 degrees azimuth /-2 degrees elevation is reflected at the 2.2 m tall metal locker.

Fig. 5 shows 3D PDPs at the BS when the Tx is located at A3. Because only the azimuth angles are considered, all the 3D PDPs due to the elevation angles are added together. Based on Fig. 5, we verify that there are many paths that exist in the indoor office environment.

Fig. 6 shows the results of peaks (paths) after detection when the Tx is located at A3. There are 54 paths coming from various directions. More specifically, from Fig. 7, we know that there are more paths for the azimuth angles around 0 degrees and +/-180 degrees compared to the other azimuth angles. By matching the azimuth arrival angles with the layout of the office, we find that these paths are reflected at wall W1 or the 2.2 m tall metal lockers and wall W1 or in the vicinity of wall W1, respectively. In particular, there are some paths that pass through the windows, are reflected by another building outside, and pass through the window again arriving at the BS. Based on Fig. 7, we also verify that most of the paths arrive with elevation angles from -10 to 10 degrees.

Fig. 8 shows the path loss depending on the Tx location. From these results, we verify that the coefficient of $log_{10}(d)$ of the measured path loss is 10.1 and is less than the coefficient of the path loss in free space.

Table II gives the number of paths, path loss, delay spread, and angle spread depending on the Tx location. Based on the table, we verify that the delay spread is less than 79 ns. The azimuth angle spread and elevation angle spread vary from 45 to 86 degrees and 0 to 12 degrees, respectively. Moreover, the averages of the delay spread, azimuth angle spread, and elevation angle spread are 60.4 ns, 64.7 degrees, and 3.6 degrees, respectively. The standard deviations of the delay spread, azimuth angle spread, and elevation angle spread are 9.7 ns, 10.7 degrees, and 3.1 degrees, respectively.

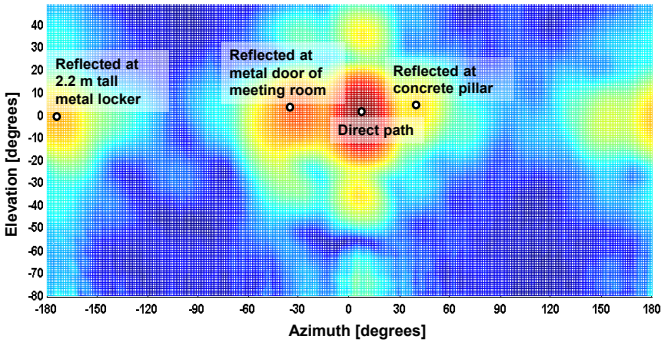

Fig. 4. Received power at BS corresponding to each combination of azimuth/elevation angle when Tx is located at A3.

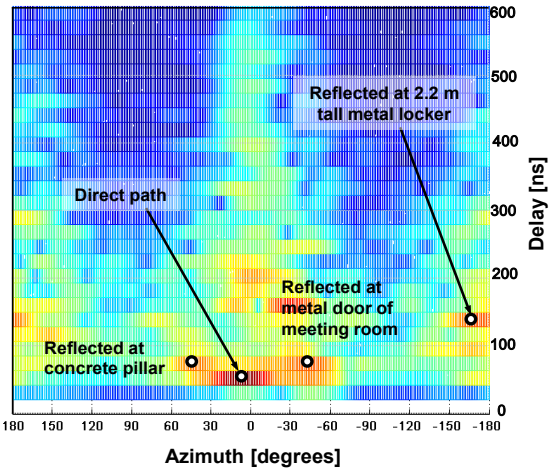

Fig. 5. 3D PDPs at BS when Tx is located at A3.

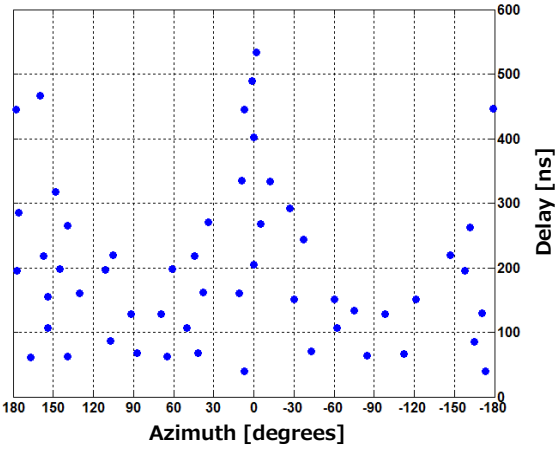

Fig. 6. Results of paths after detection when Tx is located at A3.

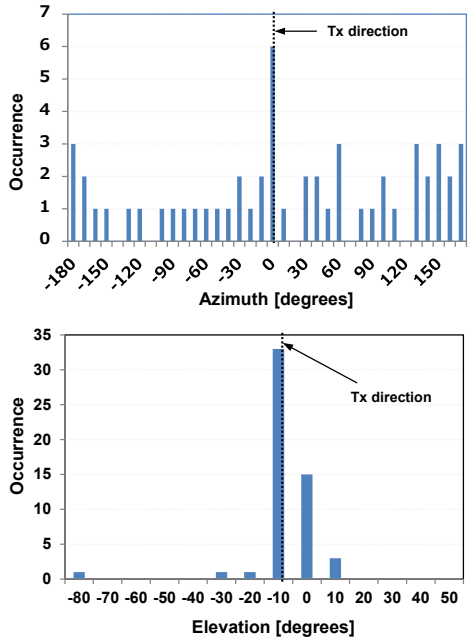

Fig. 7. Distribution of AoA when Tx is located at A3.

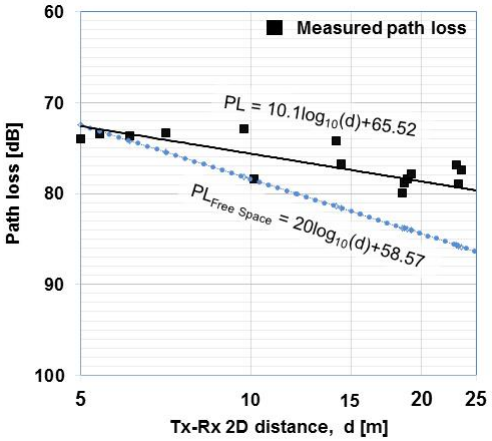

Fig. 8. Path losses depending on Tx location.

V. CONCLUSION

In this paper, we measured the indoor channel characteristics at the 20 GHz band using a channel sounder. By rotating a horn antenna in azimuth and elevation on the receiver side, we obtained the channel characteristics as if we used an omni-directional antenna. The measured and estimated results show that the path loss is less than that in free space. The averages of the delay spread, azimuth angle spread, and elevation angle spread are 60.4 ns, 64.7 degrees, and 3.6 degrees, respectively. The standard deviations of the delay spread, azimuth angle spread, and elevation angle spread are 9.7 ns, 10.7 degrees, and 3.1 degrees, respectively. In the future, we plan to estimate cluster characteristics and propose a channel model for an indoor office environment.

TABLE II. PATH LOSS, ANGLE SPREAD, AND DELAY SPREAD AT EACH TX LOCATION

TX@	Tx-Rx distance [m]	Number of paths	Measured path loss [dB]	Delay spread [ns]	Azimuth spread [deg.]	Elevation spread [deg.]
D1	5.00	61	74.0	62.3	61.2	5.9
A1	5.39	70	73.4	66.0	66.0	7.9
B1	6.10	72	73.7	53.3	73.2	12.2
C1	7.07	65	73.4	41.6	67.0	0.0
A2	9.71	52	72.9	49.6	53.4	3.3
B2	10.12	80	78.4	71.8	86.0	7.4
A3	14.14	54	74.3	63.2	49.6	4.7
B3	14.43	67	76.8	56.0	68.4	2.9
D4	18.50	82	79.9	78.7	68.0	1.6
A4	18.61	77	78.8	70.1	60.8	2.3
B4	18.83	70	78.4	53.7	59.3	1.8
C4	19.16	82	77.9	54.3	59.9	1.7
A5	23.09	72	76.8	54.5	45.8	1.0
B5	23.26	86	79.0	60.3	78.9	2.5
C5	23.54	80	77.3	48.9	52.8	1.4
A6	27.57	87	83.1	72.1	71.8	1.9
B6	27.72	92	82.5	69.9	78.4	2.1
Average		**74**	**-**	**60.4**	**64.7**	**3.6**
Standard deviation		**11**	**-**	**9.7**	**10.7**	**3.1**

REFERENCES

[1] H. Ishii, Y. Kishiyama, and H. Takahashi, "A novel architecture for LTE-B, C-plane/U-plane split and phantom cell concept," IEEE Globecom 2012 Workshop, December 2012.

[2] H. Xu, V. Kukshya, and T. S. Rappaport, "Spatial and temporal characteristics of 60-GHz indoor channels," IEEE Journal on Selected Areas in Communications, Vol. 20, No. 3, April 2002.

[3] K. Haneda, et al., "A statistical spatio-temporal radio channel model for large indoor environments at 60 and 70 GHz," IEEE Transactions on Antennas and Propagation, Vol. 63, No. 6, June 2015.

[4] B. Neekzad, et al., "Clustering characteristics of millimeter wave indoor channels," WCNC 2008 proceedings.

[5] M. Choi, et al., "Statistical characteristics of 60 GHz wideband indoor propagation channel," 2005 IEEE 16th International Symposium on Personal, Indoor and Mobile Radio Communications.

[6] S. Geng, et al., "Millimeter-wave propagation channel characterization for short-range wireless communications," IEEE Transactions on Vehicular Technology, Vol. 58, No. 1, January 2009.

[7] C. Liu, E. Skafidas, T.S. Pollock, and R.J. Evans, "Angle of arrival extended S-V model for the 60 GHz wireless desktop channel," The 17th Annual IEEE International Symposium on Personal, Indoor and Mobile Radio Communications (PIMRC'06).

[8] A. F. Abouraddy and S. M. Elnoubi, "Statistical modeling of the indoor radio channel at 10 GHz through propagation measurements-part I: Narrow-band measurements and modeling," IEEE Trans. Veh. Technol., vol. 49, no. 5, p., Sep. 2000.

[9] G. Janssen, et al., "Wideband Indoor Channel Measurements and BER Analysis of Frequency Selective Multipath Channels at 2.4, 4.75, and 11.5 GHz," IEEE Trans. on Communications, Vol. 44, No. 10, Oct 1996.

[10] M. Kim, et al., "Large Scale Parameters and Double-Directional Characterization of Indoor Wideband Radio Multipath Channels at 11 GHz," IEEE Transactions on Antennas and Propagation, Vol. 62, No. 1, Jan 2014.

[11] S. Hur, et al., "Synchronous channel sounder using horn antenna and indoor measurements on 28 GHz," in 2014 IEEE International Black Sea Conference on Communications and Networking (BlackSeaCom), May 2014, pp. 83–87.

[12] X. Wu, et al., "28 GHz Indoor Channel Measurements and Modelling in Laboratory Environment Using Directional Antennas," in 9th European Conference on Antennas and Propagation, EuCAP 2015.